Functional remodeling of lysosomes by type I interferon modifies host defense

Hailong Zhang[1,2,3], Abdelrahim Zoued[1,2,3], Xu Liu[1,2,3], Brandon Sit[1,2], Matthew K. Waldor[1,2,3]*

1Division of Infectious Diseases, Brigham and Women's Hospital, Boston, Massachusetts, USA

2Department of Microbiology, Harvard Medical School, Boston, Massachusetts, USA

3Howard Hughes Medical Institute, Boston, Massachusetts, USA

*Correspondence: mwaldor@research.bwh.harvard.edu

SUMMARY

The degradative activity of lysosomes is essential for cellular homeostasis and also functions in innate defense against intracellular microbes. Pathogens commonly modify lysosome and other organelle functions to promote virulence, but host factors that stimulate organelle re-modeling remain largely uncharacterized. Here, a CRISPR/Cas9 screen in intestinal epithelial cells with *Salmonella*, a prototypical intracellular bacterial pathogen, led us to discover that type I interferon (IFN-I) governs lysosome function. IFN-I signaling modified the localization, acidification, protease activity and proteomic profile of lysosomes, amplifying intracellular *Salmonella* virulence gene expression and host cell death. IFN-I promoted *in vivo Salmonella* pathogenesis not only in bone marrow-derived cells, but also in the intestinal epithelium, where *Salmonella* initiates infection. Our findings explain how a bacterial pathogen co-opts epithelial IFN-I signaling, and unveil an unexpected role for IFN-I signaling in control of lysosomal function. We propose that immune signal-induced organelle remodeling at barrier surfaces may broadly impact host defense against diverse infectious agents.

KEYWORDS

Type I interferon, Lysosome remodeling, *Salmonella* pathogenesis, Intestinal epithelium

INTRODUCTION

The innate immune system is essential for initial recognition of and defense against microbial pathogens at epithelial surfaces (Philpott et al., 2001). To counter these control mechanisms, pathogens have evolved virulence strategies to antagonize immune function (Reddick and Alto, 2014). Often these strategies involve direct manipulation of host cellular processes by bacterial factors such as secreted or injected protein effectors that disrupt immune responses and/or promote pathogen survival.

Compared to their extracellular counterparts, intracellular bacterial pathogens evade host immune surveillance and other external threats (e.g. antibiotics) by employing intricate virulence programs that enable them to enter and survive inside host cells (Hybiske and Stephens, 2008). In this niche, intracellular pathogens interact with and exploit the functions of host cell organelles to support their proliferation and virulence (Omotade and Roy, 2019). As a result of their intimate relationship with host cell organelles, intracellular pathogens have proven to be outstanding tools to probe basic eukaryotic cell biology. One model intracellular bacterium is *Salmonella enterica* serovar Typhimurium (*Stm*), a food-borne pathogen that initially invades and subsequently kills intestinal epithelial cells (IECs) before spreading systemically via circulating phagocytes (Hurley et al., 2014). A hallmark of *Stm* infection in IECs is formation of the *Salmonella*-containing vacuole (SCV), a dynamic, lysosome-like compartment that is permissive for *Stm* replication (Steele-Mortimer, 2008; Tuli and Sharma, 2019). Although *Stm*'s entry into and initial trafficking inside host cells is well-characterized, the IEC pathways that control *Stm*-induced cytotoxicity remain incompletely defined.

One striking feature of the host cytokine response to *Stm* is the induction of type I interferons (IFN-Is) (Hess et al., 1989). IFN-Is trigger intracellular anti-microbial transcriptional programs consisting of over 400 IFN-stimulated genes (ISGs). Due to the large size of the "interferome" and the complex interactions of ISGs with thousands of additional cellular proteins (Hubel et al., 2019), knowledge of the full spectrum of IFN-I-mediated changes in cellular function is incomplete. An increasing body of evidence indicates that in contrast to their canonical antiviral roles, IFN-Is sensitize the host to several intracellular bacterial pathogens, including *Stm* (Robinson et al., 2012). The molecular mechanisms that have been proposed to account for this phenotype have focused solely on the effects of IFN-I in phagocytic immune cell lineages (Dorhoi et al., 2014; Hos et al., 2017; Perkins et al., 2015).

Here, while defining the host IEC factors required for *Stm* cytotoxicity with a genome-scale CRISPR/Cas9 screen, we discovered a novel role for IFN-I signaling. Even in the absence of infection, we observed that IFN signaling modified epithelial cell lysosomal localization, pH and protease activity. Organellar proteomics revealed that at least 15 ISGs were enriched in lysosomes following IFN-I stimulation and one of these enriched ISGs, IFITM3, was found to directly impact lysosomal function. IFN-I signaling-dependent lysosomal acidification stimulated *Stm* virulence gene expression, facilitating *Stm*-mediated epithelial cell death. Moreover, epithelial IFN-I signaling promoted *Stm* pathogenesis *in vivo*. Thus, IFN-I signaling-induced lysosomal remodeling at barrier surfaces impacts host defense, even in non-immune cell subsets.

RESULTS

IFN-I signaling enhances *Stm* cytotoxicity

To identify host genes that confer resistance to *Stm* cytotoxicity, we performed a multi-round, genome-scale CRISPR/Cas9 loss-of-function screen in the human colonic epithelial cell line HT29-Cas9 (Blondel et al., 2016) (Figure 1A). The screen identified known pathways that sensitize cells to *Stm* infection, including those involved in regulation of actin dynamics (Arp2/3 and Rac), which are important in pathogen invasion (Unsworth et al., 2004; Yeung et al., 2019), along with pathways not previously linked to *Stm* virulence, such as the Fc-gamma receptor-dependent phagocytic and GPI anchor modification pathways (Table S1 and Figures S1A, B). Strikingly, the top enriched sgRNAs from both screened libraries represented the entire type I IFN (IFN-I) signaling pathway, including the receptor (IFNAR1/2), adaptor (JAK1/TYK2), and transcription factor (STAT1/2/IRF9) components of the system (Figures 1B, C). *Stm* induces IFN-I production during infection (Hess et al., 1989), and IFN-I signaling in immune cells such as macrophages has been identified as a host susceptibility factor for *Stm* (Robinson et al., 2012), but the contribution of IFN-I signaling in IECs is unknown. A clonal knockout of *Ifnar2*, the top enriched hit in both libraries, was constructed in the HT29-Cas9 cell line (Figure S1C), to confirm the screen findings. At both early and late infection time points, *Ifnar2* KO cells were more resistant to *Stm*-induced cell death than the wild-type (WT) parental line (Figures 1D and S1D, E). Priming cells with IFNβ (a major IFN-I), conditions which mimic the multiple rounds of the original screen, further sensitized WT but not *Ifnar2* KO cells to death (Figure 1D). We next tested whether IFN-I-promoted death depended on SPI-1 or

SPI-2, critical *Salmonella* pathogenicity islands that each encode type 3 secretion systems (T3SS) required for cellular invasion and intracellular survival, respectively (Galan et al., 2014). SPI-1-deficient (*ΔprgH*) *Stm* did not induce cell death in any condition, confirming that cytotoxicity in IECs requires cell invasion. SPI-2-deficient (*ΔssaV*) *Stm* led to reduced but still detectable levels of cytotoxicity that remained sensitive to IFNβ priming, suggestive of both SPI-2-dependent and independent mechanisms of cytotoxicity (Figure 1D). Treatment with the JAK inhibitors ruxolitinib and pyridone-6 also blocked *Stm*-induced death in WT cells, indicating active IFN-I signaling is required for this phenotype (Figure S1F). Flow cytometry of HT29 or HeLa cells infected with fluorescent *Stm* and stained with the cell death probe Annexin-V indicated that IFN-I only influenced cell death in the population of cells that contained intracellular *Stm* (Figures 1E and S1G-I). IFN-I signaling did not impact *Stm* invasion (Figures 1F and S1J), nor did it influence bacterial association with the early endosomal marker Rab5, late endosomal marker Rab7 or lysosomal marker LAMP1 (Desjardins et al., 1994) (Figures 1G, H and S1K-N). Thus, we hypothesized that IFN-I-mediated sensitization of epithelial cells to *Stm* occurs downstream of cell invasion and initial SCV formation.

IFN-I controls lysosome localization and function

During our investigation of SCV formation in IFNβ-treated cells, we unexpectedly observed that even in the absence of infection, IFN-I signaling impacts epithelial cell lysosomal localization and function. In HeLa cells, lysosomes (identifiable as LAMP1+/Lysotracker+ co-staining organelles) were scattered throughout the cytoplasm under basal conditions.

However, following IFNβ stimulation, lysosomes re-localized to the perinuclear region (Figures 2A, B); lysosome re-localization was not observed in *Ifnar2* KO HeLa cells, confirming that this response was dependent on IFN-I signaling. Furthermore, IFNβ priming led to significantly higher intensity of two fluorescent reporters (Lysotracker and Lysosensor) of lysosomal pH in WT but not *Ifnar2* KO cells, indicating that IFN-I signaling lowers lysosomal pH (Figures 2C and S2A-C). The activity of most resident lysosomal proteins, like cathepsins and other degradative enzymes, is positively regulated by acidic pH (Butor et al., 1995). Staining with fluorescent reporters of general lysosomal protease activity (DQ-BSA (Reis et al., 1998)), or cathepsin D (a major lysosomal protease) activity revealed that their activities were elevated by IFNβ stimulation in an *Ifnar2*-dependent fashion (Figures 2D, E and S2D). Importantly, IFNβ-induced lysosomal acidification and protease activation was abolished by the addition of the v-ATPase inhibitor bafilomycin A1 (Bfa1) (Yoshimori et al., 1991) (Figures 2C, D), demonstrating that IFN-I signaling primarily relies on the conventional lysosomal acidification machinery. IFN-I did not impact dextran uptake, suggesting that IFN-I signaling does not impact general endocytic trafficking (Figure S2E). Together, these observations reveal that IFN-I signaling promotes epithelial cell lysosomal relocalization, acidification and degradative activity, even in the absence of infection. IFNβ treatment also reduced lysosomal pH in monocyte/macrophage-like THP-1 cells (Figure S2F), suggesting that IFN-I signaling controls lysosomal acidification in additional cell lineages.

The ISG IFITM3 regulates lysosomal function

To investigate the mechanisms by which IFN-I modifies lysosomal function, we profiled the proteomes of intact lysosomes (Abu-Remaileh et al., 2017) purified from WT or *Ifnar2* KO cells in basal or IFNβ-stimulated states. The purity and integrity of our lysosome samples was confirmed by verifying the presence of luminal cathepsin D and absence of cytosolic and Golgi apparatus markers (Figures 3A and S3A). Quantitative profiling revealed that the abundances of ~20 proteins, most of them ISGs, were increased in purified lysosomes upon IFNβ stimulation (Figure 3B). Among these proteins was IFITM3, an IFN-induced transmembrane protein which has been shown to inhibit viral entry and has been proposed to interact with the lysosomal v-ATPase complex (Amini-Bavil-Olyaee et al., 2013; Wee et al., 2012). Concordant with the mass spectrometry analyses, IFITM3 was significantly enriched in the purified lysosomes, in contrast with IFIT3, a cytosolic ISG (Figure 3A). Immunofluorescence analysis revealed that IFITM3 co-localized with LAMP1, but not Rab5, confirming that IFITM3 is a lysosomal protein (Figure 3C).

Remarkably, lysosomal pH in *Ifitm3* KO cells was heightened in both basal and IFNβ-priming conditions relative to WT cells, partially phenocopying the *Ifnar2* KO, suggesting IFITM3 contributes to IFN-I-meditated lysosomal acidification (Figures 3D and S3B). *Ifitm3*'s contribution to basal pH levels are consistent with the tonic activities of IFNs observed in diverse mammalian cell types (Schoggins et al., 2014). Given that both lysosomal pH and degradative activity in *Ifitm3* KO cells were still somewhat sensitive to IFNβ priming (Figures 3D, E), we speculate that additional IFN-I-induced factors (including those in Figure 3B) contribute to this process.

IFN-I triggers *Stm* virulence gene expression

SPI-2 induction is linked to SCV maturation, a process that requires dynamic interactions with multiple organelles including lysosomes (Santos et al., 2015). We hypothesized that IFN-I's role in lysosomal remodeling might stimulate expression of *Stm* SPI-2-encoded and other virulence genes because reduced pH stimulates their expression (Chakraborty et al., 2015; Prost et al., 2007). Expression of SPI-1 genes, which encode invasion-specific functions, was not altered in infections with IFNβ priming or in *Ifnar2* KO cells (Figures 4A and S4A). However, IFNβ priming increased expression of SPI-2 encoded genes (Figures 4B and S4B). These genes were only induced after SCV formation (i.e. later than one-hour post infection), and the effect of IFNβ priming was eliminated in *Ifnar2* KO cells. Bfa1 treatment abolished IFNβ induction of SPI-2 expression (Figures 4B and S4B), consistent with the idea that alteration of SCV acidification is the primary mechanism of IFN-I-enhanced SPI-2 induction. Measurement of SPI-2 induction with a fluorescent P_{sifB}*::gfp* reporter strain (Garmendia et al., 2003) confirmed this phenotype at single bacterial cell resolution (Fig. 4C). Similar expression trends were observed in *Stm* acid-induced, virulence-associated genes that are not encoded within and functions independently of SPI-2 (Gunn et al., 1995) (Figures 4D and S4C, D). This is consistent with our above observation (Figure 1D) that SPI-2-deficient *Stm* retain some cytotoxicity. Together, these data indicate that IFN-I-mediated lysosomal remodeling promotes *Stm's* intracellular virulence gene expression.

The *Stm* virulence program can lead to breakage of the SCV, exposing the pathogen to the

host cytosol (Roy et al., 2004; Xu et al., 2019). In infected IFNβ-primed WT HeLa cells, ~60% of *Stm* stained positive for galectin-3, a marker of the ruptured SCV (Thurston et al., 2012), whereas <20% of *Stm* were galectin-3+ in infected *Ifnar2* KO cells (Figures 4E, F). To assess whether the pathogen was cytosol-exposed as a consequence of SCV rupture, infected cells were treated with high concentrations of gentamicin, an antibiotic that can penetrate into cells at high concentrations (Myrdal et al., 2005). *Stm* in IFNβ-treated WT cells were markedly more sensitive to gentamicin, than bacteria in IFNβ-treated *Ifnar2* KO cells (Figure 4G), suggesting that IFN-I activation of *Stm* virulence gene expression promotes SCV rupture and facilitates the pathogen's access to the cytosol. The confinement of *Stm* to the intravacuolar space in IFN-I-deficient cells could explain their protection from *Stm*-induced cytotoxicity and the identification of IFN-I signaling as a host susceptibility factor in our screen.

IFN-I promotes epithelial *Stm* pathogenesis *in vivo*

To understand the importance of IFN-I signaling in *Stm* pathogenesis, we first used a more physiologic culture system - primary human-derived small intestinal organoids. IFNβ priming of organoids increased cell death associated with *Stm* infection, whereas treatment of organoids with pyridone-6 had the opposite effect (Figures 5A, B). The absence of immune cells such as macrophages in this system supports the idea that IFN-I signaling promotes *Stm* pathogenicity in IECs.

To further dissect the importance of epithelial IFN-I signaling in the context of *in vivo Stm*

infection, we used bone marrow transfers to generate chimeric C57BL/6 mice that had *Ifnar1* deleted in only the hematopoietic compartment or in other bodily tissues, including epithelial surfaces (Figure S5A). Following intraperitoneal delivery of poly:IC to induce IFNβ production (Lauterbach et al., 2010), chimeric mice were oro-gastrically inoculated with *Stm* to assess the roles of hematopoietic and epithelial compartments in resistance to infection (Figure 5C). Mice with WT epithelia and KO bone marrow were relatively resistant to *Stm* infection, with reduced weight loss and distal organ bacterial loads compared to mice that had WT epithelia and bone marrow (Figures 5D, E), consistent with previous observations that immune cell IFN-I signaling promotes *Stm* pathogenesis (Robinson et al., 2012). Strikingly, we observed a similar phenotype in mice with KO epithelia and WT bone marrow (Figures 5D, E), suggesting that IEC IFN-I signaling also enhances *Stm* pathogenicity during infection. Mice that had both KO epithelia and bone marrow were more protected than either chimera, consistent with the idea that *Stm* takes advantage of IFN-I signaling in both the gut epithelium as well as in bone marrow-derived cells. Histological analyses revealed similar levels of tissue damage in both chimeras (Figures 5F, G); however, finer-scale immunofluorescence studies with TUNEL staining to quantify cell death showed that TUNEL+ (dying) cells tracked with the WT compartment. In *Stm*-infected chimeric mice with WT bone marrow, cell death was primarily localized to E-cadherin-negative cells in the lamina propria. In contrast, in chimeric mice with WT epithelium, TUNEL staining primarily co-localized with E-cadherin-positive IECs (Figures 5H, I). Together, these *in vivo* studies suggest that IFN-I signaling in the epithelial compartment facilitates *Stm*-induced IEC death and pathogen spread.

DISCUSSION

Our work underscores the utility of model intracellular pathogens like *Stm* as probes for the investigation of fundamental cell processes. Our initial genome-scale CRISPR/Cas9 screen revealed that IFN-I signaling sensitizes epithelial cells to *Stm* cytotoxicity, a phenotype we verified *in vitro* and *in vivo* with bone marrow chimeric mice. We found that IFN-I-dependent lysosome acidification in IECs stimulated *Stm* virulence gene expression and exacerbated cell death, offering a molecular mechanism for these observations. Strikingly, we found that infection was not necessary for IFN-I to modulate the localization, acidification and protease activity of lysosomes. In sum, by dissecting *Stm*'s interaction with the host, we identified and charted a previously unrecognized pathway by which lysosome function can be controlled.

IFN-I is widely known as an antiviral immune signal, but substantial evidence has revealed it is also a susceptibility factor for several human intracellular bacterial pathogens, including *L. monocytogenes* and *M. tuberculosis* (Auerbuch et al., 2004; Boxx and Cheng, 2016; Ji et al., 2019; O'Connell et al., 2004; Zhang et al., 2018). Studies of the bases for these phenotypes have primarily focused on immune-mediated explanations (Auerbuch et al., 2004; Dorhoi et al., 2014; Ji et al., 2019; O'Connell et al., 2004). For *Stm*, proposed mechanisms have invoked elevated macrophage necroptosis (Hos et al., 2017; Robinson et al., 2012) and transcriptional reprogramming (Perkins et al., 2015), altered dendritic cell homeostasis (Stefan et al., 2017), and increased neutrophil-mediated inflammation (Wilson et al., 2019). We propose that in addition to these immune-centric mechanisms, IFN-I-induced remodeling of epithelial cell lysosomes directly impacts the *Stm* virulence program and shapes the outcome of infection.

Our findings suggest that IFN-I signaling can modify innate defense in the epithelial as well as the immune compartment. The contribution of IFN-I modulation of lysosome function to *Stm* infection in non-epithelial cells, such as macrophages, requires further study. It remains an open question whether *Stm* purposely stimulates and exploits IFN-I signaling as part of its pathogenic strategy.

While we found that IFN-I-induced lysosomal acidification sensitizes cells to a bacterial pathogen, our finding that many other known ISGs with antiviral properties, such as IFITM3, were enriched in lysosomal proteomes from IFN-I-stimulated cells leads us to speculate that this mechanism may be protective against viral threats. IFN-I-mediated lysosomal remodeling may also play a role in non-infectious pathologies, such as lysosomal cholesterol accumulation (Kuhnl et al., 2018) and other lysosome-related disorders. It remains unclear whether these effects might be driven by the tonic IFN-I signaling that occurs in many tissues (Schoggins et al., 2014), or instead require pathogenic over-induction of IFN-I.

To our knowledge, our study provides the first evidence showing that IFN-I signaling governs the composition and function of an organelle – the lysosome. It will be of interest to determine whether other immune signals (i.e. IFN-II and other cytokines) can also direct lysosomal remodeling. Furthermore, IFNs and other cytokines may also promote the functional remodeling of other organelles, such as the mitochondria and endoplasmic reticulum, under homeostasis and in diverse pathogenic contexts. Such activities may constitute a broadly applicable lens through which to view and enhance our understanding of the cell biology of innate defense.

AUTHORCONTRIBUTIONS

H.L.Z. and M.K.W. conceived and all authors designed the study. H.L.Z., A.Z., and X.L. performed all experiments and analyzed data. H.L.Z., B.S., and M.K.W. wrote the manuscript and all authors edited the paper.

ACKNOWLEDGEMENTS

We thank members of the Waldor lab for helpful discussions on all aspects of this project, Dr. David Breault at the Harvard Digestive Diseases Center (HDDC) Organoid Core for the primary human small intestine organoids; and Michal Pyzik from Dr. Richard Blumberg's lab for assistance in creation of bone marrow chimeric mice.

Research in the M.K.W. laboratory is supported by HHMI and NIH grant R01 AI-042347. A.Z. was supported by an EMBO long-term fellowship (ALTF 1514-2016) and by a HHMI Fellowship of the Life Sciences Research Foundation.

DECLARATION OF INTERESTS

The authors declare no competing interests.

Figure 1.A genome-scale screen reveals IFN-I promotes *Stm* cytotoxicity

(A) Workflow for CRISPR/Cas9 *Stm* cytotoxicity screen in HT29-Cas9 cells.

(B) Scatterplots showing normalized reads enrichment of specific sgRNAs in two libraries (A and B) after 4 rounds of *Stm* infection. Genes involved in IFN-I signaling are delineated by the dashed red circle.

(C) Overview of IFN-I signaling pathway. Numbers correspond to hit ranks in each library.

(D) Survival of IFNβ-primed or unprimed WT or *Ifnar2* KO HT29 cells 4 hours post WT or mutant *Stm* infection. Mean ± s.d., n = 3.

(E) Flow cytometry of IFNβ-primed or unprimed WT and *Ifnar2* KO HT29 cells 20 hours post mCherry-*Stm* infection and stained with Annexin V-FITC. FITC, fluorescein isothiocyanate.

(F) Flow cytometric quantification of invasion of HT29 cells by mCherry-*Stm*. Mean ± s.d., n = 3.

(G) Representative images of LAMP1-RFP-expressing HeLa cells 4 hours post GFP-*Stm* infection. Boxed insets depict higher magnification showing bacterial colocalization with LAMP1-RFP. Scale bar, 10μm.

(H) Quantification of LAMP1-RFP-positive *Stm* from 10 fields. Mean ± s.d., n = 3.

Statistical analysis was performed by two-tailed Student's *t* test (**P < 0.01 and ***P < 0.001).

See also Figure S1 and Table S1.

Figure 2. IFN-I signaling regulates lysosomal positioning, acidity, and protease activity

(A) Representative images of lysosome (LAMP1-GFP+/LysoTracker+ compartment)

distribution in WT and *Ifnar2* KO HeLa cells with or without 16 hours of IFNβ stimulation. Nuclei (blue) were stained with DAPI and actin (purple) was stained with phalloidin. Scale bar, 5μm.

(B) Quantification of perinuclear lysosome indices from 10 cells. Mean ± s.d., n = 3.

(C-D) Flow cytometry of LysoTracker Red (C) and DQ-Green BSA fluorescence (D) in HeLa cells ±16 hours of treatment with IFNβ or the lysosomal acidification inhibitor Bfa1. Vertical dashed lines indicate the mean fluorescence value of the mock control in WT (red) or *Ifnar2* KO (blue) cells.

(E) Relative cathepsin D activity in WT and *Ifnar2* KO HeLa cells ± 16 hours of IFNβ treatment. Mean ± s.d., n = 5.

Statistical analysis was performed by two-tailed Student's *t* test (***P < 0.001).

See also Figure S2.

Figure 3. IFN-I signaling shapes the lysosomal proteome

(A) Immunoblotting for known (LAMP1, CTSD) and suspected (IFITM3) lysosomal proteins in whole-cell lysates (T) and purified lysosomes (IP).

(B) Relative fold change scatterplot of protein abundance in lysosomes purified from WT or *Ifnar2* KO HeLa cells ± 16 hours of IFNβ treatment. Colored dots indicate proteins that are known ISGs.

(C) Representative images of LAMP1-RFP or Rab5-RFP–expressing HeLa cells stained with IFITM3 antibody (GFP). Nuclei (blue) were stained with DAPI. Scale bar, 5μm.

(D-E) Flow cytometry of LysoTracker Red (D) and DQ-Green BSA fluorescence (E) in WT, *Ifitm3* KO and *Ifnar2* KO HeLa cells ± 16 hours of IFNβ treatment.

See also Figure S3.

Figure 4. IFN-I signaling promotes *Stm* virulence gene expression and SCV rupture

Relative induction of SPI-1 (*prgH*) (A), SPI-2 (*ssaV*) (B) and PhoP-induced virulence gene (*pagD*) (D) in intracellular *Stm* from WT and *Ifnar2* KO HeLa cells ± 16 hours of drug treatment. Data are normalized to transcript levels in LB-cultured *Stm* (red). Mean ± s.d., n = 3.

(C) Flow cytometry of intracellular P_{sifB}*::gfp Stm* isolated from WT and *Ifnar2* KO HeLa cells ± 16 hours of drug treatment. LB-cultured *Stm* were used as the mock control.

(E) Representative images of Gal3-GFP-expressing HeLa cells 4 hour post mCherry-*Stm* infection. Scale bar, 10μm.

(F) Quantification of the Gal3 positive SCVs from 10 cells. Mean ± s.d., n = 3.

(G) Intracellular CFU counts from IFNβ-treated WT and *Ifnar2* KO HeLa cells 2 hour post *Stm* infection. Infected cells were treated with gentamicin (Gm) at the indicated concentrations (μg/ml). Data were normalized to the WT+IFNβ Gm 10 group. Mean ± s.d., n = 5.

Statistical analysis was performed by two-tailed Student's *t* test (***P < 0.001).

See also Figure S4 and Table S2.

Figure 5. IFN-I signaling in intestinal epithelial cells promotes *Stm* pathogenesis.

(A) Representative images of IFNβ or pyridone-6-primed or unprimed human small bowel

enteroids 20 hours post WT *Stm* infection. Propidium iodide (PI) staining was used to detect cell death. Scale bar, 100 μm.

(B) Enteroid survival 20 hours post WT *Stm* infection. Mean ± s.d., n = 3.

(C) Timeline of generation (top) and oral *Stm* infection (bottom) of *Ifnar1* chimeric mice.

(D) Body weights of *Stm*-infected chimeric mice. Mean ± s.e.m., n = 12 mice.

(E) Liver and spleen *Stm* CFU burdens from chimeric mice 5 days post-*Stm* infection. Mean ± s.d., n = 12 mice.

(F) Representative H&E stained ileal sections from chimeric mice 5 days post-*Stm* infection. Scale bars, 100μm.

(G) Average histological scores of chimeric mice 5 days post-*Stm* infection from 8 fields. Mean ± s.d., n = 4 mice.

(H) Representative images of ileal sections from chimeric mice 5 days post-*Stm* infection. IECs were identified with E-cadherin (red), dying cells with TUNEL (green), and nuclei with DAPI (blue). The white dashed line marks the epithelial surface. Scale bar, 100μm.

(I) Quantification of TUNEL+/E-cadherin+ (red) or TUNEL+/E-cadherin- (blue) cells per field from 8 fields. Mean ± s.d., n = 4 mice.

Statistical analysis was performed by two-tailed Student's *t* test in (B) and (G). Statistical analysis was performed by two-tailed Mann-Whitney U-test in (D) and (E). (*P < 0.05, **P < 0.01 and ***P < 0.001).

See also Figure S5.

Figure S1. IFN-I promotes *Stm* cytotoxicity but not affect *Stm* invasion and SCV maturation, Related to Figure 1

(A) Adjusted p values for selected enriched Gene Ontology (GO) terms from GO-analyzed hits in the *Stm* cytotoxicity screen (upper threshold set at $p < 1E-03$).

(B) Cytoscape visualization of enriched pathways.

(C) Relative expression of the IFN-I target gene *oas1* in WT and *Ifnar2* KO HT29 cells 16 hours post-IFNβ treatment. Mean ± s.d., n = 3.

(D) Survival of IFNβ-primed or unprimed WT or *Ifnar2* KO HT29 cells 20 hours post WT or mutant *Stm* infection. Mean ± s.d., n = 3.

(E) Representative bright-field images of WT and *Ifnar2* KO HT29 cells 2 days post *Stm* infection. Scale bar, 250 μm or 100 μm, respectively.

(F)Survival of mock or drug-treated WT HT29 cells 20 hours post WT *Stm* infection. Mean ± s.d., n = 3.

(G) Quantification of flow cytometry data in Figure 1E. Mean ± s.d., n = 4.

(H) Flow cytometry of IFNβ-primed or unprimed WT and *Ifnar2* KO HeLa cells 20 hours post mCherry-*Stm* infection and stained with Annexin V-FITC.

(I) Quantification of flow cytometry data from Figure S1F. Mean ± s.d., n = 4.

(J) Flow cytometry of IFNβ-primed WT and *Ifnar2* KO HT29 cells 4 hours post mCherry-*Stm* infection. Quantification is shown in Figure 1F.

(K) Representative images of Rab5-RFP-expressing HeLa cells at 4 hours post GFP-*Stm* infection. Scale bar, 10 μm.

(L) Quantification of Rab5-RFP-positive *Stm* from 10 fields. Mean ± s.d., n = 3.

(M) Representative images of Rab7-RFP-expressing HeLa cells 4 hours post GFP-*Stm* infection. Scale bar, 10 μm.

(N) Quantification of Rab7-RFP-positive *Stm* from 10 fields. Mean ± s.d., n = 3.

Statistical analysis was performed by two-tailed Student's *t* test (*P < 0.05, **P < 0.01 and ***P < 0.001).

Figure S2. IFN-I signaling regulates lysosomal acidity, protease activity in both epithelial cell and THP1 cells, but not impact endocytic trafficking, Related to Figure 2

(A) Quantification of mean fluorescence intensity (MFI) from Figure 2C. Mean ± s.d., n = 3.

(B) Flow cytometry of LysoSensor staining in WT and *Ifnar2* KO HeLa cells ± 16 hours of IFNβ treatment.

(C) Flow cytometry of LysoTracker staining in HT29 cells ± 16 hours of drug treatment.

(D) Quantification of mean fluorescence intensity from Figure 2D. Mean ± s.d., n = 3.

(E) Flow cytometry of Dextran-568 uptake in WT and *Ifnar2* KO HeLa cells ± 16 hours of IFNβ treatment.

(F) Flow cytometry of LysoTracker staining in monocytic macrophage-like THP1 cells ± 16 hours of IFNβ treatment.

Statistical analysis was performed by two-tailed Student's *t* test (**P < 0.01 and ***P < 0.001).

Figure S3. Purity of isolated lysosomes and IFITM3 gene KO in HeLa cells, Related to Figure 3

(A) Immunoblotting for protein markers of indicated subcellular compartments in whole-cell lysates (T) and purified lysosomes (IP).

(B) Immunoblotting for IFITM3 in WT and *Ifitm3* KO HeLa cells ± 16 hours of IFNβ treatment.

Figure S4. Intracellular *Stm* virulence gene expression, Related to Figure 4

(A-D) Relative induction of individual SPI-1 (A), SPI-2 (B), PhoP-induced (C) or SPI-3 (D) genes in intracellular *Stm* from WT and *Ifnar2* KO HeLa cells ± drug treatment. Data are normalized to transcript levels from LB-cultured *Stm* (red). Mean ± s.d., n = 3.

Statistical analysis was performed by two-tailed Student's *t* test (***P < 0.001).

Figure S5. Generation of chimeric mice by bone marrow transfer, Related to Figure 5

(A-C) Flow cytometry of peripheral blood CD45.1 and CD45.2+ cells in mock and chimeric mice 4 weeks after bone marrow transplantation. WT mock mice carry CD45.2 allele but not CD45.1 (A), which is totally abolished by irradiation (B, C). 4 weeks later after CD45.1 BM transfer, the chimeric mice carry CD45.1 allele but not CD45.2 (B, C).

STAR METHODS

KEY RESOURCE TABLE

REAGENT or RESOURCE	SOURCE	IDENTIFIER
Antibodies		
LAMP1 (D4O1S) Mouse mAb	Cell Signaling Technology	15665S
Anti-IFIT3/P60 antibody [OTI1G1]	Abcam	ab118045
IFITM3 Antibody	Proteintech	11714-1-AP
Cathepsin D Monoclonal Antibody (CTD-19)	ThermoFisher	MA1-26773
Anti-GM130 antibody [EP892Y] - cis-Golgi Marker	Abcam	ab52649
β-Actin Antibody (AC-15)	Santa Cruz	sc-69879
PE/Cy7 anti-mouse CD45.2	Biolegend	109829
FITC anti-mouse CD45.1	Biolegend	110706
Human/Mouse E-Cadherin Antibody	R&D	AF748
Anti-Rabbit IgG (whole molecule)–Peroxidase antibody	Sigma	A4914
Goat anti-Mouse IgG (H+L) Secondary Antibody, HRP	ThermoFisher	31430
Rabbit anti-Goat IgG (H+L) Cross-Adsorbed Secondary Antibody, HRP	Invitrogen	R-21459
Donkey anti-Goat IgG (H+L) Cross-Adsorbed Secondary Antibody, Alexa Fluor 568	Invitrogen	A-11057
Goat anti-Rabbit IgG (H+L) Highly Cross-Adsorbed Secondary Antibody, Alexa Fluor 488	Invitrogen	A-11034
Bacterial Strains		
Salmonella Typhimurium SL1344	Dr. Dirk Bumann	
Salmonella Typhimurium SL1344 ΔprgH	This study	
Salmonella Typhimurium SL1344 ΔssaV	This study	
Salmonella Typhimurium SL1344-eGFP	This study	
Salmonella Typhimurium SL1344-mCherry	This study	
Salmonella Typhimurium SL1344-P_{sifB}-GFP	Dr. Dirk Bumann	
Salmonella Typhimurium SL1344-mCherry-P_{sifB}-GFP	This study	
One Shot Stbl3 Chemically Competent E. coli	Thermo Fisher Scientific	Cat No.C737303
Chemicals and Recombinant Proteins		
IFNβ	Peprotech	Cat No. 300-02BC
pyridine-6	BioVision	Cat No. 2534
Ruxolitinib (NCB018424)	Selleckchem	Cat No.S1378
Polybrene,	Sigma	Cat No. TR-1003-G
Trizol	Invitrogen	Cat No. 15596018

SuperScript III reverse transcriptase	Invitrogen	Cat No. 18080085
Roche 2×SYBR master mix	Roche	Cat No. 04707516001
BfA1	SantaCruz	Cat No. sc-201550
Critical Commercial Assays		
Blood and Cell Culture DNA MaxiKit	QIAGEN	Cat No. 13362
TransIT-LT1	Mirus	Cat No. MIR230
QIAquick Gel Extraction Kit	Qiagen	Cat No. 28704
LDH assay kit	Promega	Cat No. G1780
FITC Annexin V Apoptosis Detection kit	BioLegend	Cat No. 640922
Lipofectamine 3000	ThermoFisher	Cat No. L3000008
Lysotracker	ThermoFisher	Cat No. L7528
Lysosensor	Thermofisher	Cat No. L7545
fluorogenic peptide substrate of cathepsin D	Biovision	Cat No. K143
Dextran 568	ThermoFisher	Cat No. D22912
DQ-Red BSA	ThermoFisher	Cat No. D12050
10% Tris-Glycine gels	ThermoFisher	Cat No. XP00102BOX
nitrocellulose membranes	Invitrogen	Cat No. IB23002
SuperSignal West Pico Enhanced Chemiluminescence kit	ThermoFisher	Cat No. 34577
PureLink Micro-to-Midi total RNA purification system	Invitrogen	Cat No. 12183
Ambion Turbo DNA-free DNase	Invitrogen	Cat No. AM1907
TUNEL kit	ThermoFisher	Cat No. A23210
Experimental Models: Cell Lines		
HeLa	ATCC	CRM-CCL-2, female
HEK293T	ATCC	CRL-3216, female
HT29	ATCC	HTB-38, female
THP-1	ATCC	TIB-202, male
Primary human small intestine organoids	Harvard Digestive Diseases Center Organoid Core	Gift from Dr. David Breault
Experimental Models: Organisms/Strains		
Mouse: C57BL/6J B6(Cg)-Ifnar1tm1.2Ees/J	The Jackson Laboratory	Stock No: 028288
Mouse: B6.SJL-Ptprca Pepcb/BoyJ	The Jackson Laboratory	Stock No: 002014
Oligonucleotides		
qPCR primers, see Table S3		
CRISPR gene KO primers, see Table S4		

Recombinant DNA		
lentiGuide-Puro	Addgene	52963
psPAX2	Addgene	12260
pMD2.G	Addgene	12259
pLJC5-LAMP1-RFP-3xHA	Addgene	102932
pHR-FKBP:mCherry-Rab5a	Addgene	72901
pHR-FKBP:mCherry-Rab7a	Addgene	72903
LAMP1-mGFP	Addgene	34831
pLJC5-Tmem192-3xHA	Addgene	102930
mAG-GAL3	Addgene	62734
Software and Algorithms		
Primer3	Untergasser et al., 2012	http://primer3.ut.ee/
ImageJ	NIH	https://imagej.nih.gov/ij/download.html
FlowJo 10.2	FlowJo	https:/www.flowjo.com/solutions/flowjo.
GraphPad Prism	GraphPad Software	https://www.graphpad.com.
Gene set enrichment Analysis	Broad Institute	http://www.broadinstitute.org/gsea.
DAVID analysis	NIAID/NIH	http://david.abcc.ncifcrf.gov

CONTACT FOR REAGENT AND RESOURCE SHARING

Further information and requests for resources and reagents should be directed to and will be fulfilled by the Lead Contact, Matthew K Waldor (mwaldor@research.bwh.harvard.edu)

EXPERIMENTAL MODEL AND SUBJECT DETAILS

Bacterial strains, plasmids, and antibodies

Strains, plasmids, oligonucleotides and antibodies used in this study are listed in key resources

table and table S3, 4. *Escherichia coli* K-12 DH5α λ pir was used for cloning procedures and plasmid propagation. *S. typhimurium* strain SL1344 and its ΔSPI-1 and ΔSPI-2 derivatives were cultured in Luria-Bertani (LB) medium or on LB agar plates at 37°C supplemented with streptomycin (100μg/ml). The SPI-1 (*prgH*) and SPI-2 (*ssaV*) genes were deleted from wild-type (WT) SL1344 with the lambda red recombination system (Datsenko and Wanner, 2000). This approach was also used to introduce the GFP and mCherry-coding sequence with a constitutive promoter (P_{rpsM}) into the *putP-putA* locus (Hautefort et al., 2003).

Cell lines

HeLa (ATCC, Cat No. CRM-CCL-2, female) and HEK293T (ATCC, Cat No. CRL-3216, female) cells were cultured in Dulbecco's modified Eagle's medium (DMEM; ThermoFisher, Cat No. 11965) supplemented with 10% fetal bovine serum (FBS; Gibco, Cat No. 16140-071). HT29 (ATCC, Cat No. HTB-38, female) cells were cultured in McCoy's 5A modified medium (Thermo Fisher, Cat No. 30-2007) supplemented with 10% FBS. THP-1 (ATCC, Cat No. TIB-202, male) cells were cultured in RPMI-1640 medium (Lonza, Cat No. 12-167F) with 10% non-heat inactivated FBS (GeminiBio, Cat NO. 100-500) and supplemented with HEPES (Lonza, Cat No. 17-737E), 2-Mercaptoethanol (Invitrogen, Cat No. 21985023) and L-Glutamine (Lonza, Cat No. 17-605E). All cells were cultured at 37°C in a 5% CO_2 incubator.

Infection of organoids derived from human small intestine

Primary human small intestine organoids (enteroids) were kindly provided by Dr. David Breault at the Harvard Digestive Diseases Center (HDDC) Organoid Core. Enteroids were cultured in the following medium: advanced DMEM/F12 (Gibco, Cat No.12634-028) supplemented with L-WRN conditioned medium (ATCC CRL-3276; HDDC Organoids Core), HEPES (10mM, pH 7.4), GlutaMax (Gibco, Cat No.35050-061), B_{27} (Gibco, Cat No.12587010), N2 (Gibco, Cat No.17502-048), 1mM N-acetyl-L-cysteine (Sigma, Cat No.A8199), 10mM nicotinamide (Sigma, Cat No.N0636), 5µM A83-01 (Sigma, Cat No.SML0788), 10µM SB202190 (Sigma, Cat No.S7067), 50ng/ml murine EGF (Peprotech, Cat No.315-09), 10nM gastrin (Sigma, Cat No.G9145), and 10µM Y-27632 (Sigma, Cat No.Y0503). For *Stm* infection, approximately 100 enteroids were seeded in 50µl Matrigel (Corning, Cat No.356231) in each well of a 24-well plate. Three to four days after seeding, enteroids were either mock treated, or primed with either 10ng/ml IFNβ or 0.5 µM pyridine-6 for 16 hours. Enteroids were then released from Matrigel by incubation in 500µl Cell Recovery Solution (Corning, Cat No.354253) for 30 mins on ice. Resuspended enteroids were pipetted up and down 50 times with a P1000 pipette and then transferred to a new 24-well plate. Each well was infected with approximately 3×10^7 *Stm*. The plate was centrifuged for 5 mins at 300× g before it was placed in a 37°Cincubator for 30 mins. After infection, enteroids were transferred to microcentrifuge tubes, spundown, mixed with 50µl Matrigel per tube/sample, and seeded into a new 24-well plate. After Matrigel solidification at 37°C, 500µl full enteroid media containing 50µg/ml gentamicin was added to each well at 10ng/ml IFNβ or 0.5µM pyridine-6 was added to the corresponding primed samples. At 20 hpi, propidium iodide (Invitrogen, Cat No.V13241) was used to stain the

enteroids before imaging. To quantitatively measure cell death, the media from each well/sample was also assayed for LDH activity as described above. LDH release values of mock treated samples were set at 1 for normalization.

Bone marrow chimera mice

C57BL/6 and *Ifnar1*$^{-/-}$ mice were purchased from The Jackson Laboratory (Bar Harbor, ME, USA) and were maintained on a 12-hour light/dark cycle and a standard chow diet at the Harvard Institute of Medicine specific pathogen-free (SPF) animal facility (Boston, MA, USA). Animal experiments were performed according to guidelines from the Center for Animal Resources and Comparative Medicine at Harvard Medical School. All protocols and experimental plans were approved by the Brigham and Women's Hospital Institutional Animal Care and Use Committee (Protocol #2016N000416). Littermate control male and female mice were randomly assigned to each group and experiments were performed blinded with respect to treatment. For bone marrow chimeras, recipient mice were irradiated two times with 600 rad 1 day before injection of bone marrow from WT or *Ifnar1*$^{-/-}$ mice. Bone marrow was extracted from femurs of donor mice by flushing with PBS and then washed once in PBS; 1×10^6 cells were injected into the tail vein of recipient mice. Mice were monitored for 4 weeks, at which point engraftment was evaluated by flow cytometry.

Infection of chimeric mice

20μg poly (I:C) (Sigma, Cat No. P1530) was given intraperitoneally to chimeric mice one day

before *Stm* infection and every other day for a total of 3 doses to stimulate IFN production. Food was withdrawn for 4 hours before infection. *Stm* inocula were prepared as described above. Mice were infected orogastrically with 5×10^8 *Stm* in 100µl PBS. Food was returned to the cages 2hpi. Infected mice were sacrificed 5 days after infection. Tissue samples of the small intestine, spleen and liver were collected for histological analysis and enumeration of colony-forming units (CFU). CFU were quantified by serial-dilution plating of homogenized tissue samples on LB plates containing 100µg/ml streptomycin.

METHOD DETAILS

Pharmacologic inhibitors and IFNβ priming

JAK inhibitors pyridine-6 (BioVision, Cat No. 2534) and ruxolitinib (NCB018424) (Selleckchem, Cat No.S1378) were used at 0.5µM. IFNβ (Peprotech, Cat No. 300-02BC) was used at 10ng/ml for cell priming. Drug-treated cells were primed for 16 hours (unless otherwise indicated) before *Stm* infection.

Stm infections

All tissue culture infections were done according to the following procedure unless otherwise indicated. WT and mutant *Stm* were grown for ~16 hours at 37°C with shaking and then sub-cultured (1:33) in LB without antibiotics for 3 hours until the cultures reached an OD_{600} of 0.8.To prepare the inoculum, cultures were first pelleted at 5,000× g for 5 min. The pellets were

resuspended in DMEM without FBS, and an appropriate volume of bacterial solution was added to cells to reach a multiplicity of infection (MOI) of 100 bacteria per eukaryotic cell. The cells were then incubated with bacteria for 30 min at 37°C with 5% CO_2. Extracellular bacteria were removed by extensive washing with phosphate-buffered saline (PBS; Gibco, Cat No. 14190250) and addition of 50µg/ml gentamicin to the medium. At 2 hours post infection (hpi), the gentamicin concentration was decreased to 5µg/ml.

CRISPR/Cas9 *Stm* infection screen

HT29-Cas9 CRISPR libraries were constructed as described previously (Blondel et al., 2016) using the Avana sgRNA library, which contains four different sgRNAs targeting each human protein-coding gene (Doench et al., 2016). For each library, two sets of four T225 flasks (Corning, Cat No. 14-826-80) were seeded with 15×10^6 cells per flask and then incubated for 48 hours. At the time of the screen, there were ~150×10^6 cells per experimental condition, corresponding to ~2,000× coverage per sgRNA. Cells were at ~70% confluence at the time of infection. The infection was done as described above with minor modifications. Briefly, HT29 libraries were infected with WT *Stm* at an MOI of 300 for 30 min. After infection, the libraries were expanded in McCoy's 5A + FBS containing 5µg/ml gentamicin, to both permit intracellular bacterial cytotoxicity and minimizethe intracellular gentamicin concentration to allow *Stm* invasion during the next round of infection. Flasks were checked daily to monitor recovery of survivor cells; when 70% confluency was achieved, cells were trypsinized, pooled, and reseeded for the next round of infection. In total, four rounds of infection were conducted.

Surviving cells from the last round of infection were used for preparation of genomic DNA.

Genomic DNA preparation, sequencing, and analyses of screen results

Genomic DNA was obtained from 75× 10^6 cells after positive selection, as well as from input cells, using the Blood and Cell Culture DNA MaxiKit (QIAGEN, Cat No. 13362). sgRNA sequences was amplified by PCR as described (Doench et al., 2016). The read counts were first normalized to reads per million within each condition by the following formula: reads per sgRNA / total reads per condition × 10^6. Reads per million were then log_2-transformedby first adding 1 to all values, in order calculate the log of sgRNAs with zero reads. The log_2 fold-change of each sgRNA was then determined relative to the input sample for each biological replicate. MAGeCK analysis for genome-scale CRISPR-Cas9 knockout screens was used to evaluate the rank and statistical significance of perturbations from the ranked list (Li et al., 2014) and enriched pathways were determined using ClueGo (Bindea et al., 2009).

Lentivirus preparation and transductions

The Galectin 3, Rab5, Rab7, LAMP1, and LC3B lentiviral expression plasmids used in the study are listed in Table S4. Lentiviral packaging plasmids psPAX2 and pVSV-G, and the corresponding cargo plasmid were transfected into 293T cells with the TransIT-LT1 transfection reagent (Mirus, Cat No. MIR230). 48 hours following transfection, 293T culture supernatants were harvested, passed through a 0.45µm pore filter, and added to target cells that were grown to 70-80% confluency in 6-well plates. Polybrene (Sigma, Cat No. TR-1003-G) (8µg/ml) was

added and the 6-well plates were spun at 1000×g for 2 hours at 30°C, after which cells were returned to 37°C. The infections were repeated the next day with supernatants from 72 hour-transfected 293T cultures.

Construction of cell lines with targeted gene disruptions

The sgRNA sequences used for construction of targeted HT29-Cas9 and HeLa-Cas9 mutant cell lines are listed in Table S4. All sgRNA oligonucleotides were obtained from Integrated DNA Technologies (IDT) and cloned into the pLentiGuide-Puro plasmid. Briefly, 5µg of plasmid pLentiGuide-Puro was digested with BmsBI (Fermentas, Cat No. ER0451) and purified using the QIAquick Gel Extraction Kit (Qiagen, Cat No. 28704). Each pair of oligos was annealed and phosphorylated with T4 PNK (NEB, Cat No. M0201S) in the presence of 10× T4 DNA ligase buffer in a thermocycler with the following parameters: i) incubation for 30 minutes at 37°C, ii) incubation at 95°C for 5 min with a ramp down to 25°C at 5°C per minute. Oligos were then diluted 1:200, and 1µl of the diluted oligo mixture was ligated with 50ng of BsmBI digested plasmid. Ligations were transformed into the STBL3 *Escherichia coli* strain (Thermo Fisher, Cat No. C7373-03) and positive clones were identified by Sanger sequencing (Genewiz). Lentiviral transduction of sgRNAs cloned into pLentiGuide-Puro into HT29-Cas9 and HeLa-Cas9 cells was performed as described above. Targeted gene KO cell lines were selected by puromycin (1µg/ml) for 10 days. HT29 KO cells were isolated as single clones while HeLa cells were CRISPR KO pools after drug selection.

Cell survival assays

For cell survival assays, 5×10^4 HT29 cells were seeded into 96-well plates and primed with or without drugs in McCoy's 5Amedium supplemented with 10% FBS.HT29 cells were infected with *Stm*s trains at an MOI of 100 as described above. Cell survival analysis was performed using an LDH assay (Promega, Cat No. G1780) according to the manufacturer's protocol at 4 and 20 hpi.

***Stm* invasion assays**

mCherry-or GFP-tagged *Stm* were used in all flow cytometry and immunofluorescence experiments. *Stm* infections were performed as described above with varying MOIs. At 4hpi, suspended and attached cells were collected, resuspended in PBS, and immediately analyzed with a LSR II (BD Bioscience) or SH800 (Sony) flow cytometer. Data were processed with FlowJo software (v10.6.1).

Annexin V staining and FACS analysis

Cell death was detected with the FITC Annexin V Apoptosis Detection kit (BioLegend, Cat No. 640922). Infections were performed as described above with mCherry-*Stm* at an MOI of 100. 20 hpi suspended and attached cells were collected, resuspended in 100μl of Annexin V binding buffer at 1×10^7 cells/ml and mixed with 5μl of FITC-conjugated Annexin V. After incubation at room temperature (RT) for 15 min in the dark, 400μl of Annexin V binding buffer was added and stained cells were immediately analyzed by flow cytometry as described above.

Immunofluorescence microscopy of tissue cultured cells

HeLa cells were seeded in 12-well plates on 18 mm glass coverslips or 6-well chambers (Mat-TEK, Cat No.P06G-1.5-10-F). Cells were transiently transfected with LAMP1-GFP expressing plasmid mixed with Lipofectamine 3000 (ThermoFisher, Cat No. L3000008) according to the manufacturer's instructions. 24 hours post-transfection cells were primed with or without 10ng/ml IFNβ for 16 hours.The cells were then stained with 75nM Lysotracker (ThermoFisher, Cat No. L7528) for 15 min and then fixed with 2% PFA for 20 min at RT. The samples were washed with PBS three times, and stained with fluorescent phalloidin (1:1000) and 4,6-diamidino-2-phenylindole (DAPI, 1 μg /ml) to label actin filaments and nuclei, respectively. For experiments with LAMP1-RFP, Rab5-RFP, Rab7-RFP, Gal3-GFP, and eGFP-LC3B cell lines, cells were seeded in 6-well chambers and primed with 10ng/ml IFNβ for 16 hours before infection with fluorescently-labeled *Stm* at an MOI 50. Live cells were analyzed at 2 hpi by confocal microscopy to detect localization of Gal3 and *Stm*.

Quantification of lysosome distribution

Lysosome distribution was analyzed as described (Li et al., 2016); the area occupied by nuclei was excluded from analyses. Average LAMP1 intensities were measured for the area within 5μm of the nucleus ($I_{perinuclear}$), and the area >10μm from the nucleus ($I_{peripheral}$). The average intensities were calculated and normalized to cell areas. The perinuclear index was defined as $I_{perinuclear}$ /$I_{peripheral}$. Quantifications were carried out on10 cells per group with ImageJ.

Measurement of lysosome acidity

Cells with no treatment or with either 10ng/ml IFNβ or 5nM BfA1 (SantaCruz, Cat No. sc-201550) treatment for 16 hours were stained with 75nM Lysotracker or Lysosensor (Thermofisher, Cat No. L7545) for 15 min and washed with PBS. The fluorescence intensity of the stained cells was determined by flow cytometry.

Cathepsin D activity assay

HeLa cells were seeded in 96-well plates with or without 10ng/ml IFNβ priming for 16 hours. A fluorogenic peptide substrate of cathepsin D, Mca-P-L-G-L-Dpa-A-R-NH2 (Biovision, Cat No. K143), was added to the cells to a final concentration of 200μM for 2 hours. The fluorescence intensity of each well was measured with a fluorescence plate reader. Each sample was assayed in triplicate and normalized to a standard curve.

Endocytosis and lysosome function assays

HeLa cells were seeded in 24-well plates with or without 10ng/ml IFNβ priming. Cells were treated with either 50μg/ml Dextran 568 (ThermoFisher, Cat No. D22912) or 25μg/ml DQ-Red BSA (ThermoFisher, Cat No. D12050) for 2 hours in growth medium. Then, cells were washed with PBS and trypsinized for fluorescence quantification by flow cytometry.

Lysosome immunopurification (LysoIP)

LysoIP was performed largely as described (Abu-Remaileh et al., 2017). Briefly, pLJC5-3×HA-TMEM192 was used to introduce a lysosomal tag protein in WT and *Ifnar2* KO HeLa cells. 15 million cells were used for each replicate. Cells were rinsed twice with pre-chilled PBS and then scraped in 1ml of PBS containing protease and phosphatase inhibitors and pelleted at 100×g for 2 min at 4°C. Cells were resuspended in 950µl of the same buffer, and 25µl (equivalent to 2.5% of the total number cells) was reserved for further processing to generate the whole-cell sample. The remaining cells were gently homogenized with 25 strokes of a 2ml Dounce-type homogenizer. The homogenate was then centrifuged at 100×g for 2 min at 4°C to pellet the cell debris and intact cells, while cellular organelles including lysosomes remained in the supernatant. The supernatant was incubated with 150µl of anti-HA magnetic beads preequilibrated with PBS on a rotator shaker for 3 min. Immunoprecipitates were then gently washed three times with PBS on a DynaMag Spin Magnet. Beads with bound lysosomes were resuspended in 100µl pre-chilled 1% Triton-X lysis buffer to extract proteins. After 10 min incubation on ice, the beads were removed with the magnet. 5µl of each sample were subjected to 12.5%-acrylamide SDS-PAGE and immunodetected using antibody listed in Table S6, while the remainder was submitted to the Thermo Fisher Center for Multiplexed Proteomics of Harvard Medical School (Boston, MA, USA) for Isobaric Tandem Mass Tag (TMT)-based quantitative proteomics.

Immunoblot analyses

Mammalian cell lysates were prepared in radioimmuno-precipitation assay (RIPA) buffer

supplemented with 1 tablet of EDTA-free protease inhibitor (Roche, Cat No. C762Q77) per 25ml buffer. Lysates were kept at 4°C for 30 min and then clarified by centrifugation in a microcentrifuge at 13,000 rpm at 4°C for 10 min. Proteins were denatured by the addition of SDS sample buffer and boiling for 5 min. Proteins were separated by electrophoresis in 10% Tris-Glycine gels (ThermoFisher, Cat No. XP00102BOX), and then transferred onto nitrocellulose membranes (Invitrogen, Cat No. IB23002). The antibodies and dilutions used are listed in Table S6. Blots were developed with the SuperSignal West Pico Enhanced Chemiluminescence kit (ThermoFisher, Cat No. 34577), and imaged with a Chemidoc (Bio-Rad).

qRT-PCR quantification of *Stm* virulence gene expression

Hela cells were seeded at 1.5×10^6 cells per 6-well plates. After drug-treatment for 16 hours, cells were infected with *Stm* at an MOI of 50 as described above. Cells were washed with PBS and lysed in Trizol (Invitrogen, Cat No. 15596018) at 1and 4 hpi. RNA was purified with the PureLink Micro-to-Midi total RNA purification system (Invitrogen, Cat No. 12183) according to the manufacturer's instructions. RNA samples were treated for residual DNA contamination using Ambion Turbo DNA-free DNase (Invitrogen, Cat No. AM1907). Purified RNA was quantified on a Nanodrop 1000 (Thermo Scientific). RNA was reverse transcribed for quantitative RT-PCR (qRT-PCR) experiments by adding 10µg of total RNA to a mixture containing random hexamers (Life Technologies), 0.01M dithiothreitol, 25 mM dNTPs (Thermo Scientific, Cat No. R0191), reaction buffer and 200 units of SuperScript III reverse

transcriptase (Invitrogen, Cat No. 18080085). cDNA was diluted 1:50 in dH_2O and mixed with an equal volume of target-specific primers and Roche 2×SYBR master mix (Roche, Cat No.04707516001). Plates were centrifuged at 1000 rpm for 1 min and stored at 4°C in the dark until ready for use. Primer pairs were designed to minimize secondary structures, a length of ~20-nucelotides and a melting temperature of 60°C using the primer design software Primer 3. Primer sequences are listed in Table S3. For data normalization, quadruplicate C_t values for each sample were averaged and normalized to C_t values of the control gene *rpoB*. The relative gene expression level of *Stm* in infection conditions was normalized to LB-cultured *Stm*.

Flow cytometric analysis of *Stm* virulence gene expression

HeLa cells were infected with mCherry-and *sifB*-GFP-expressing-*Stm* as described above. Cell lysis was performed 4 hpi by washing three times with PBS and subsequent incubation for 10 min with PBS containing 0.1% Triton X-100. Cell lysates were then analyzed by flow cytometry. *Stm* were first identified by gating on the mCherry signal and *sifB* expression was quantified by gating on the mCherry+/GFP+ population. LB cultured *Stm* served as negative control.

Gentamicin protection assay

Gentamicin protection assays were carried out as described (Knodler et al., 2014). Briefly, HeLa cells in 96-well plates were infected in triplicate with *Stm* at an MOI of 50. Cells were washed three times with PBS and incubated in medium containing 100µg/ml gentamicin for 30

min to eliminate extracellular bacteria. Then, media with either 10, 100 or 400µg/ml gentamicin was applied to the cells. Cells were lysed 2hpi by washing three times with PBS and subsequent incubation for 10 min with PBS containing 0.1 % Triton X-100. Colony forming units (CFUs) were enumerated by plating serial dilutions of the lysates onto LB plates with 100µg/ml streptomycin. Data was normalized to the CFU of WT HeLa cells at gentamicin 10.

Histology and tissue immunofluorescence

Formalin-fixed, paraffin-embedded distal small intestinal samples sections of 4µm thickness were mounted on glass slides and stained with hematoxylin and eosin. Histology score was evaluated as described (Erben et al., 2014). For immunofluorescence analysis, distal small intestinal samples were collected and flushed with PBS and fixed in 4% paraformaldehyde (PFA) overnight at 4°C followed by washing with PBS. Tissues were embedded in Optimal Cutting Temperature Compound (Tissue-Tek) and stored at -80°C before sectioning on a CM1860 UV cryostat (Leica). 6µm-thick slides were stained with TUNEL (ThermoFisher, Cat No. A23210) according to the manufacturer's instructions and then incubated with anti-E-cadherin antibodies at 4°C overnight at a 1:200 in PBS. The next day, AF568-conjugated secondary antibody, diluted at 1:500, was applied to the slides for 1 hour. Nuclei were stained with DAPI at RT for 5 min in the dark. Samples were imaged with an Eclipse Ti confocal microscope with a 20×□objective (Nikon).

QUANTIFICATION AND STATISTICAL ANALYSIS

Statistical analyses were carried out using the two-tailed Student's *t* test or one-way analysis of variance (ANOVA) with Dunnet's post-correction on GraphPad Prism5.

DATA AND CODE AVAILABILITY

Original data for results of CRISPR screening is in Table S1, and original data for mass spectrometry of lysosome proteomic is in Table S2.

Supplementary items

Table S1: CRISPR/Cas9 screening results, related to figure 1

Table S2: Mass spectrometry of lysosome proteomic, related to figure 3

Table S3: qPCR primers

Table S4: CRISPR KO primers

REFERENCES

Abu-Remaileh, M., Wyant, G.A., Kim, C., Laqtom, N.N., Abbasi, M., Chan, S.H., Freinkman, E., and Sabatini, D.M. (2017). Lysosomal metabolomics reveals V-ATPase- and mTOR-dependent regulation of amino acid efflux from lysosomes. Science *358*, 807-813.

Amini-Bavil-Olyaee, S., Choi, Y.J., Lee, J.H., Shi, M., Huang, I.C., Farzan, M., and Jung, J.U. (2013). The antiviral effector IFITM3 disrupts intracellular cholesterol homeostasis to block viral entry. Cell host & microbe *13*, 452-464.

Auerbuch, V., Brockstedt, D.G., Meyer-Morse, N., O'Riordan, M., and Portnoy, D.A. (2004). Mice lacking the type I interferon receptor are resistant to Listeria monocytogenes. J Exp Med *200*, 527-533.

Bindea, G., Mlecnik, B., Hackl, H., Charoentong, P., Tosolini, M., Kirilovsky, A., Fridman, W.H., Pages, F., Trajanoski, Z., and Galon, J. (2009). ClueGO: a Cytoscape plug-in to decipher functionally grouped gene ontology and pathway annotation networks. Bioinformatics *25*, 1091-1093.

Blondel, C.J., Park, J.S., Hubbard, T.P., Pacheco, A.R., Kuehl, C.J., Walsh, M.J., Davis, B.M., Gewurz, B.E., Doench, J.G., and Waldor, M.K. (2016). CRISPR/Cas9 Screens Reveal Requirements for Host Cell Sulfation and Fucosylation in Bacterial Type III Secretion System-Mediated Cytotoxicity. Cell host & microbe *20*, 226-237.

Boxx, G.M., and Cheng, G. (2016). The Roles of Type I Interferon in Bacterial Infection. Cell host & microbe *19*, 760-769.

Butor, C., Griffiths, G., Aronson, N.N., Jr., and Varki, A. (1995). Co-localization of hydrolytic enzymes with widely disparate pH optima: implications for the regulation of lysosomal pH. J Cell Sci *108 (Pt 6)*, 2213-2219.

Chakraborty, S., Mizusaki, H., and Kenney, L.J. (2015). A FRET-based DNA biosensor tracks OmpR-dependent acidification of Salmonella during macrophage infection. PLoS biology *13*, e1002116.

Datsenko, K.A., and Wanner, B.L. (2000). One-step inactivation of chromosomal genes in Escherichia coli K-12 using PCR products. Proc Natl Acad Sci U S A *97*, 6640-6645.

Desjardins, M., Celis, J.E., van Meer, G., Dieplinger, H., Jahraus, A., Griffiths, G., and Huber, L.A. (1994). Molecular characterization of phagosomes. J Biol Chem *269*, 32194-32200.

Doench, J.G., Fusi, N., Sullender, M., Hegde, M., Vaimberg, E.W., Donovan, K.F., Smith, I., Tothova, Z., Wilen, C., Orchard, R.*, et al.* (2016). Optimized sgRNA design to maximize activity and minimize off-target effects of CRISPR-Cas9. Nat Biotechnol *34*, 184-191.

Dorhoi, A., Yeremeev, V., Nouailles, G., Weiner, J., 3rd, Jorg, S., Heinemann, E., Oberbeck-Muller, D., Knaul, J.K., Vogelzang, A., Reece, S.T.*, et al.* (2014). Type I IFN signaling triggers immunopathology in tuberculosis-susceptible mice by modulating lung phagocyte dynamics. Eur J Immunol *44*, 2380-2393.

Erben, U., Loddenkemper, C., Doerfel, K., Spieckermann, S., Haller, D., Heimesaat, M.M., Zeitz, M., Siegmund, B., and Kuhl, A.A. (2014). A guide to histomorphological evaluation of intestinal inflammation in mouse models. Int J Clin Exp Pathol *7*, 4557-4576.

Galan, J.E., Lara-Tejero, M., Marlovits, T.C., and Wagner, S. (2014). Bacterial type III secretion systems: specialized nanomachines for protein delivery into target cells. Annual review of microbiology *68*, 415-438.

Garmendia, J., Beuzon, C.R., Ruiz-Albert, J., and Holden, D.W. (2003). The roles of SsrA-SsrB and OmpR-EnvZ in the regulation of genes encoding the Salmonella typhimurium SPI-2 type III secretion system. Microbiology *149*, 2385-2396.

Gunn, J.S., Alpuche-Aranda, C.M., Loomis, W.P., Belden, W.J., and Miller, S.I. (1995). Characterization of the

784 Salmonella typhimurium pagC/pagD chromosomal region. J Bacteriol *177*, 5040-5047.
785 Hautefort, I., Proenca, M.J., and Hinton, J.C. (2003). Single-copy green fluorescent protein gene fusions allow
786 accurate measurement of Salmonella gene expression in vitro and during infection of mammalian cells. Appl
787 Environ Microbiol *69*, 7480-7491.
788 Hess, C.B., Niesel, D.W., and Klimpel, G.R. (1989). The induction of interferon production in fibroblasts by invasive
789 bacteria: a comparison of Salmonella and Shigella species. Microb Pathog *7*, 111-120.
790 Hos, N.J., Ganesan, R., Gutierrez, S., Hos, D., Klimek, J., Abdullah, Z., Kronke, M., and Robinson, N. (2017). Type I
791 interferon enhances necroptosis of Salmonella Typhimurium-infected macrophages by impairing antioxidative
792 stress responses. J Cell Biol *216*, 4107-4121.
793 Hubel, P., Urban, C., Bergant, V., Schneider, W.M., Knauer, B., Stukalov, A., Scaturro, P., Mann, A., Brunotte, L.,
794 Hoffmann, H.H.*, et al.* (2019). A protein-interaction network of interferon-stimulated genes extends the innate
795 immune system landscape. Nature immunology *20*, 493-502.
796 Hurley, D., McCusker, M.P., Fanning, S., and Martins, M. (2014). Salmonella-host interactions - modulation of the
797 host innate immune system. Front Immunol *5*, 481.
798 Hybiske, K., and Stephens, R.S. (2008). Exit strategies of intracellular pathogens. Nat Rev Microbiol *6*, 99-110.
799 Ji, D.X., Yamashiro, L.H., Chen, K.J., Mukaida, N., Kramnik, I., Darwin, K.H., and Vance, R.E. (2019). Type I
800 interferon-driven susceptibility to Mycobacterium tuberculosis is mediated by IL-1Ra. Nat Microbiol *4*, 2128-2135.
801 Knodler, L.A., Nair, V., and Steele-Mortimer, O. (2014). Quantitative assessment of cytosolic Salmonella in
802 epithelial cells. PLoS One *9*, e84681.
803 Kuhnl, A., Musiol, A., Heitzig, N., Johnson, D.E., Ehrhardt, C., Grewal, T., Gerke, V., Ludwig, S., and Rescher, U.
804 (2018). Late Endosomal/Lysosomal Cholesterol Accumulation Is a Host Cell-Protective Mechanism Inhibiting
805 Endosomal Escape of Influenza A Virus. mBio *9*.
806 Lauterbach, H., Bathke, B., Gilles, S., Traidl-Hoffmann, C., Luber, C.A., Fejer, G., Freudenberg, M.A., Davey, G.M.,
807 Vremec, D., Kallies, A.*, et al.* (2010). Mouse CD8alpha+ DCs and human BDCA3+ DCs are major producers of
808 IFN-lambda in response to poly IC. J Exp Med *207*, 2703-2717.
809 Li, W., Xu, H., Xiao, T., Cong, L., Love, M.I., Zhang, F., Irizarry, R.A., Liu, J.S., Brown, M., and Liu, X.S. (2014).
810 MAGeCK enables robust identification of essential genes from genome-scale CRISPR/Cas9 knockout screens.
811 Genome Biol *15*, 554.
812 Li, X., Rydzewski, N., Hider, A., Zhang, X., Yang, J., Wang, W., Gao, Q., Cheng, X., and Xu, H. (2016). A molecular
813 mechanism to regulate lysosome motility for lysosome positioning and tubulation. Nat Cell Biol *18*, 404-417.
814 Myrdal, S.E., Johnson, K.C., and Steyger, P.S. (2005). Cytoplasmic and intra-nuclear binding of gentamicin does not
815 require endocytosis. Hear Res *204*, 156-169.
816 O'Connell, R.M., Saha, S.K., Vaidya, S.A., Bruhn, K.W., Miranda, G.A., Zarnegar, B., Perry, A.K., Nguyen, B.O., Lane,
817 T.F., Taniguchi, T.*, et al.* (2004). Type I interferon production enhances susceptibility to Listeria monocytogenes
818 infection. J Exp Med *200*, 437-445.
819 Omotade, T.O., and Roy, C.R. (2019). Manipulation of Host Cell Organelles by Intracellular Pathogens.
820 Microbiology spectrum *7*.
821 Perkins, D.J., Rajaiah, R., Tennant, S.M., Ramachandran, G., Higginson, E.E., Dyson, T.N., and Vogel, S.N. (2015).
822 Salmonella Typhimurium Co-Opts the Host Type I IFN System To Restrict Macrophage Innate Immune
823 Transcriptional Responses Selectively. Journal of immunology *195*, 2461-2471.
824 Philpott, D.J., Girardin, S.E., and Sansonetti, P.J. (2001). Innate immune responses of epithelial cells following

825 infection with bacterial pathogens. Current opinion in immunology *13*, 410-416.
826 Prost, L.R., Daley, M.E., Le Sage, V., Bader, M.W., Le Moual, H., Klevit, R.E., and Miller, S.I. (2007). Activation of the
827 bacterial sensor kinase PhoQ by acidic pH. Mol Cell *26*, 165-174.
828 Reddick, L.E., and Alto, N.M. (2014). Bacteria fighting back: how pathogens target and subvert the host innate
829 immune system. Mol Cell *54*, 321-328.
830 Reis, R.C., Sorgine, M.H., and Coelho-Sampaio, T. (1998). A novel methodology for the investigation of intracellular
831 proteolytic processing in intact cells. Eur J Cell Biol *75*, 192-197.
832 Robinson, N., McComb, S., Mulligan, R., Dudani, R., Krishnan, L., and Sad, S. (2012). Type I interferon induces
833 necroptosis in macrophages during infection with Salmonella enterica serovar Typhimurium. Nature immunology
834 *13*, 954-962.
835 Roy, D., Liston, D.R., Idone, V.J., Di, A., Nelson, D.J., Pujol, C., Bliska, J.B., Chakrabarti, S., and Andrews, N.W. (2004).
836 A process for controlling intracellular bacterial infections induced by membrane injury. Science *304*, 1515-1518.
837 Santos, J.C., Duchateau, M., Fredlund, J., Weiner, A., Mallet, A., Schmitt, C., Matondo, M., Hourdel, V.,
838 Chamot-Rooke, J., and Enninga, J. (2015). The COPII complex and lysosomal VAMP7 determine intracellular
839 Salmonella localization and growth. Cell Microbiol *17*, 1699-1720.
840 Schoggins, J.W., MacDuff, D.A., Imanaka, N., Gainey, M.D., Shrestha, B., Eitson, J.L., Mar, K.B., Richardson, R.B.,
841 Ratushny, A.V., Litvak, V.*, et al.* (2014). Pan-viral specificity of IFN-induced genes reveals new roles for cGAS in
842 innate immunity. Nature *505*, 691-695.
843 Steele-Mortimer, O. (2008). The Salmonella-containing vacuole: moving with the times. Curr Opin Microbiol *11*,
844 38-45.
845 Stefan, K.L., Fink, A., Surana, N.K., Kasper, D.L., and Dasgupta, S. (2017). Type I interferon signaling restrains
846 IL-10R+ colonic macrophages and dendritic cells and leads to more severe Salmonella colitis. PLoS One *12*,
847 e0188600.
848 Thurston, T.L., Wandel, M.P., von Muhlinen, N., Foeglein, A., and Randow, F. (2012). Galectin 8 targets damaged
849 vesicles for autophagy to defend cells against bacterial invasion. Nature *482*, 414-418.
850 Tuli, A., and Sharma, M. (2019). How to do business with lysosomes: Salmonella leads the way. Curr Opin
851 Microbiol *47*, 1-7.
852 Unsworth, K.E., Way, M., McNiven, M., Machesky, L., and Holden, D.W. (2004). Analysis of the mechanisms of
853 Salmonella-induced actin assembly during invasion of host cells and intracellular replication. Cell Microbiol *6*,
854 1041-1055.
855 Wee, Y.S., Roundy, K.M., Weis, J.J., and Weis, J.H. (2012). Interferon-inducible transmembrane proteins of the
856 innate immune response act as membrane organizers by influencing clathrin and v-ATPase localization and
857 function. Innate Immun *18*, 834-845.
858 Wilson, R.P., Tursi, S.A., Rapsinski, G.J., Medeiros, N.J., Le, L.S., Kotredes, K.P., Patel, S., Liverani, E., Sun, S., Zhu, W.*,*
859 *et al.* (2019). STAT2 dependent Type I Interferon response promotes dysbiosis and luminal expansion of the
860 enteric pathogen Salmonella Typhimurium. PLoS Pathog *15*, e1007745.
861 Xu, Y., Zhou, P., Cheng, S., Lu, Q., Nowak, K., Hopp, A.K., Li, L., Shi, X., Zhou, Z., Gao, W.*, et al.* (2019). A Bacterial
862 Effector Reveals the V-ATPase-ATG16L1 Axis that Initiates Xenophagy. Cell *178*, 552-566 e520.
863 Yeung, A.T.Y., Choi, Y.H., Lee, A.H.Y., Hale, C., Ponstingl, H., Pickard, D., Goulding, D., Thomas, M., Gill, E., Kim, J.K.*,*
864 *et al.* (2019). A Genome-Wide Knockout Screen in Human Macrophages Identified Host Factors Modulating
865 Salmonella Infection. mBio *10*.

866 Yoshimori, T., Yamamoto, A., Moriyama, Y., Futai, M., and Tashiro, Y. (1991). Bafilomycin A1, a specific inhibitor of
867 vacuolar-type H(+)-ATPase, inhibits acidification and protein degradation in lysosomes of cultured cells. J Biol
868 Chem *266*, 17707-17712.
869 Zhang, G., deWeerd, N.A., Stifter, S.A., Liu, L., Zhou, B., Wang, W., Zhou, Y., Ying, B., Hu, X., Matthews, A.Y.*, et al.*
870 (2018). A proline deletion in IFNAR1 impairs IFN-signaling and underlies increased resistance to tuberculosis in
871 humans. Nat Commun *9*, 85.

872

873

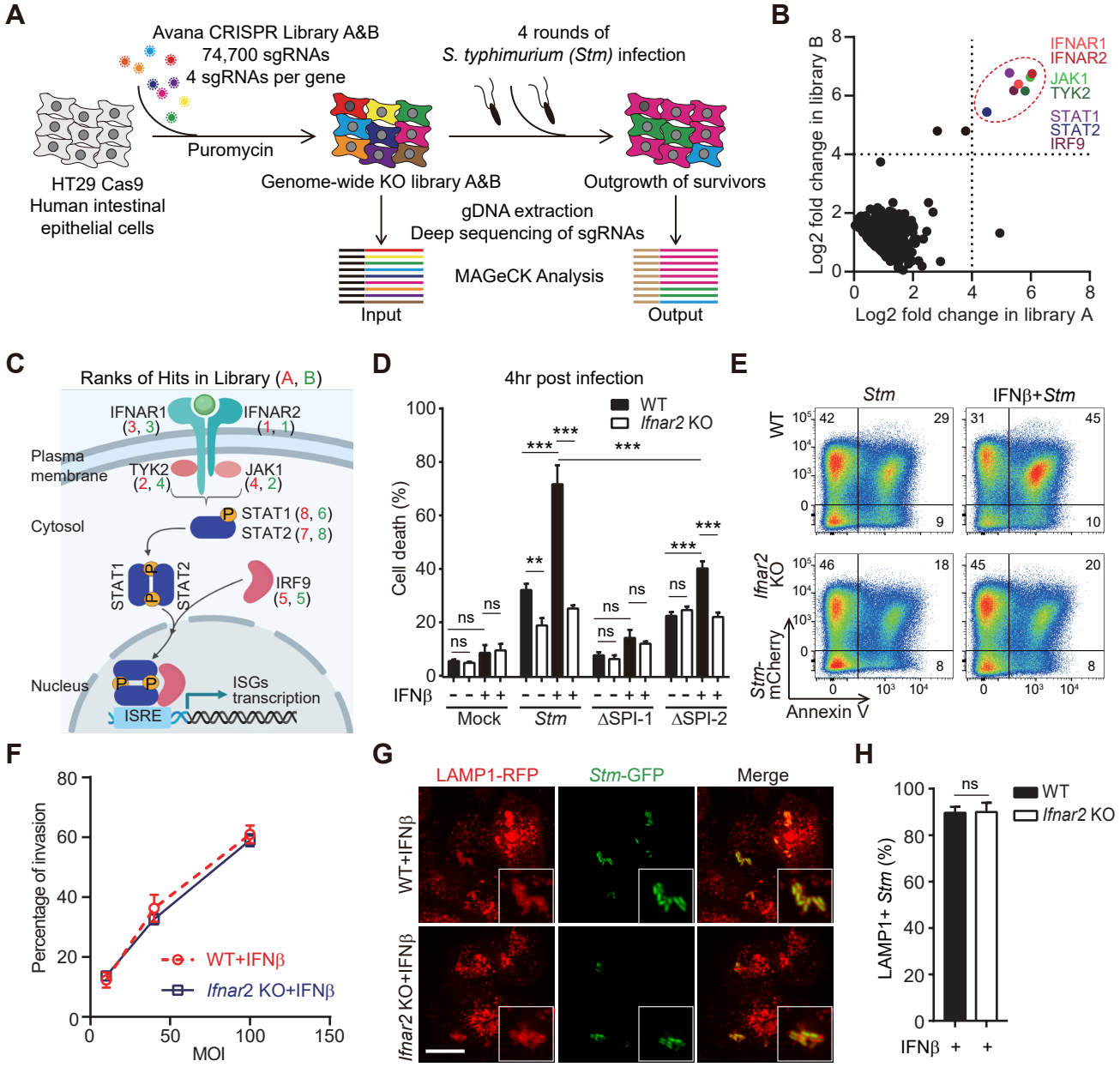
A
Avana CRISPR Library A&B
74,700 sgRNAs
4 sgRNAs per gene
4 rounds of
S. typhimurium (Stm) infection
Puromycin
HT29 Cas9
Human intestinal
epithelial cells
Genome-wide KO library A&B
Outgrowth of survivors
gDNA extraction
Deep sequencing of sgRNAs
MAGeCK Analysis
Input
Output
B
Log2 fold change in library B
Log2 fold change in library A
IFNAR1
IFNAR2
JAK1
TYK2
STAT1
STAT2
IRF9
C
Ranks of Hits in Library (A, B)
IFNAR1 (3, 3)
IFNAR2 (1, 1)
Plasma membrane
TYK2 (2, 4)
JAK1 (4, 2)
Cytosol
STAT1 (8, 6)
STAT2 (7, 8)
IRF9 (5, 5)
Nucleus
ISGs transcription
ISRE
D
4hr post infection
WT
Ifnar2 KO
Cell death (%)
IFNβ
Mock
Stm
ΔSPI-1
ΔSPI-2
E
Stm
IFNβ+Stm
WT
Ifnar2 KO
Stm-mCherry
Annexin V
F
Percentage of invasion
MOI
WT+IFNβ
Ifnar2 KO+IFNβ
G
LAMP1-RFP
Stm-GFP
Merge
WT+IFNβ
Ifnar2 KO+IFNβ
H
LAMP1+ Stm (%)
WT
Ifnar2 KO
IFNβ

Figure. 1

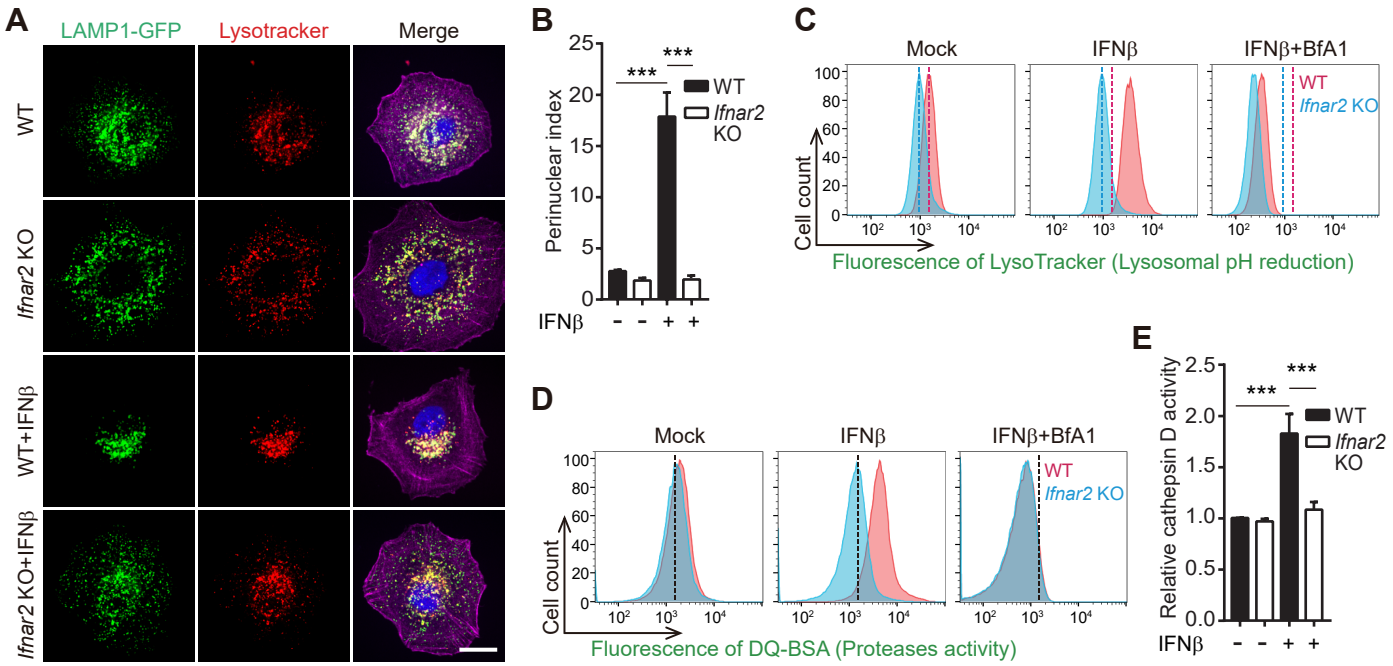
A
LAMP1-GFP
Lysotracker
Merge
WT
Ifnar2 KO
WT+IFNβ
Ifnar2 KO+IFNβ
B
Perinuclear index
***
***
WT
Ifnar2 KO
IFNβ
- - + +
C
Mock
IFNβ
IFNβ+BfA1
WT
Ifnar2 KO
Cell count
Fluorescence of LysoTracker (Lysosomal pH reduction)
D
Mock
IFNβ
IFNβ+BfA1
WT
Ifnar2 KO
Cell count
Fluorescence of DQ-BSA (Proteases activity)
E
Relative cathepsin D activity
***
***
WT
Ifnar2 KO
IFNβ
- - + +

Figure. 2

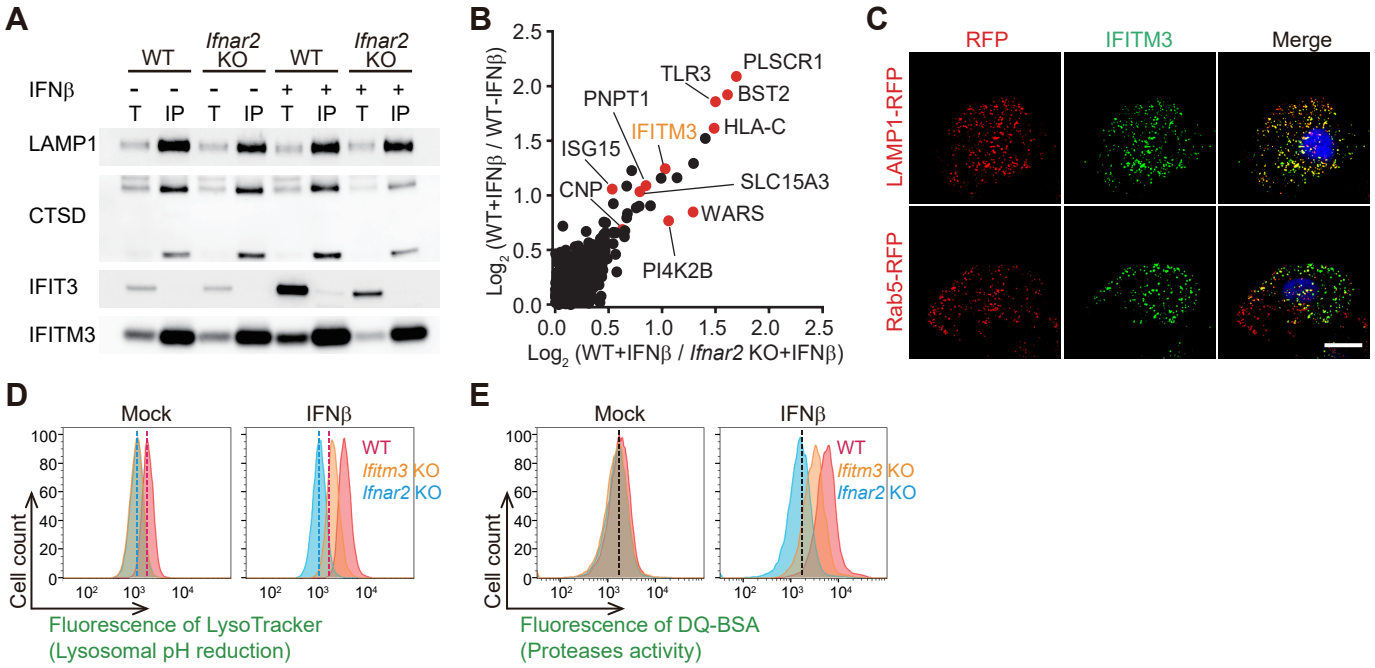
A
WT
Ifnar2 KO
WT
Ifnar2 KO
IFNβ
- - - - + + + +
T IP T IP T IP T IP
LAMP1
CTSD
IFIT3
IFITM3
B
Log2 (WT+IFNβ / WT-IFNβ)
Log2 (WT+IFNβ / Ifnar2 KO+IFNβ)
PLSCR1
TLR3
BST2
PNPT1
HLA-C
IFITM3
ISG15
SLC15A3
CNP
WARS
PI4K2B
C
RFP
IFITM3
Merge
LAMP1-RFP
Rab5-RFP
D
Mock
IFNβ
WT
Ifitm3 KO
Ifnar2 KO
Cell count
Fluorescence of LysoTracker
(Lysosomal pH reduction)
E
Mock
IFNβ
WT
Ifitm3 KO
Ifnar2 KO
Cell count
Fluorescence of DQ-BSA
(Proteases activity)

Figure. 3

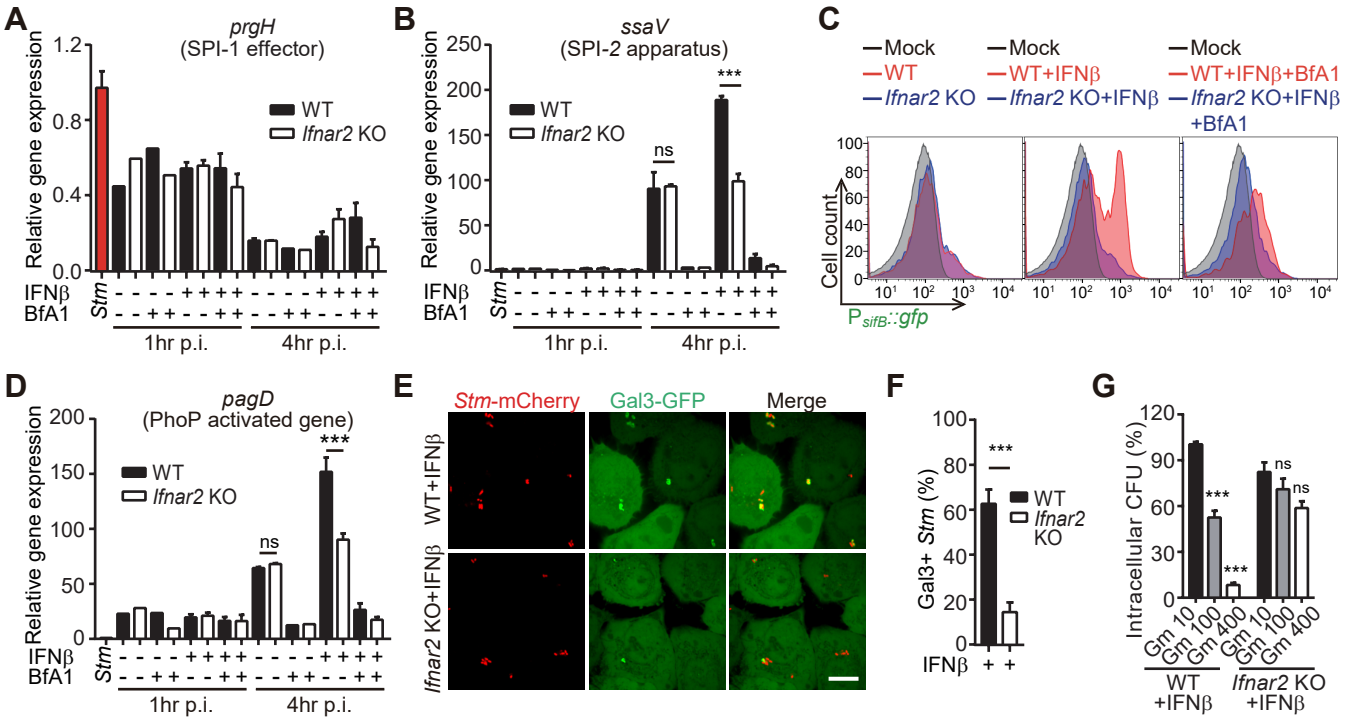
A
prgH
(SPI-1 effector)
Relative gene expression
WT
Ifnar2 KO
IFNβ
BfA1
Stm
1hr p.i.
4hr p.i.
B
ssaV
(SPI-2 apparatus)
ns
***
C
Mock
WT
Ifnar2 KO
WT+IFNβ
Ifnar2 KO+IFNβ
WT+IFNβ+BfA1
Ifnar2 KO+IFNβ +BfA1
Cell count
PsifB::gfp
D
pagD
(PhoP activated gene)
E
Stm-mCherry
Gal3-GFP
Merge
WT+IFNβ
Ifnar2 KO+IFNβ
F
Gal3+ Stm (%)
G
Intracellular CFU (%)
Gm 10
Gm 100
Gm 400
WT +IFNβ
Ifnar2 KO +IFNβ

Figure. 4

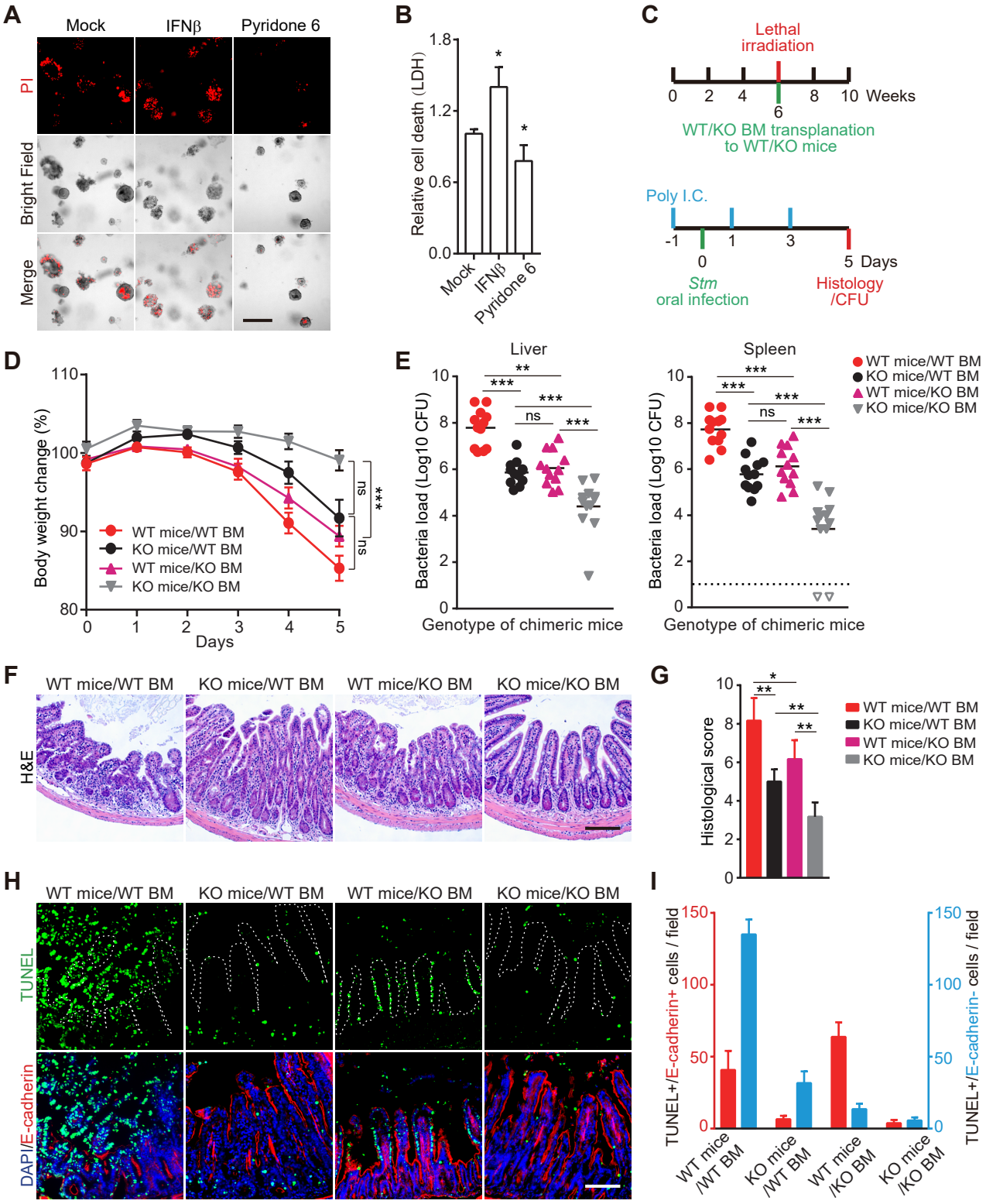
A
Mock
IFNβ
Pyridone 6
PI
Bright Field
Merge
B
Relative cell death (LDH)
1.8
1.2
0.6
0.0
Mock
IFNβ
Pyridone 6
C
Lethal irradiation
0 2 4 6 8 10 Weeks
WT/KO BM transplanation to WT/KO mice
Poly I.C.
-1 0 1 3 5 Days
Stm oral infection
Histology /CFU
D
Body weight change (%)
Days
WT mice/WT BM
KO mice/WT BM
WT mice/KO BM
KO mice/KO BM
ns
***
E
Liver
Spleen
Bacteria load (Log10 CFU)
Genotype of chimeric mice
WT mice/WT BM
KO mice/WT BM
WT mice/KO BM
KO mice/KO BM
F
WT mice/WT BM
KO mice/WT BM
WT mice/KO BM
KO mice/KO BM
H&E
G
Histological score
H
TUNEL
DAPI/E-cadherin
I
TUNEL+/E-cadherin+ cells / field
TUNEL+/E-cadherin- cells / field
WT mice /WT BM
KO mice /WT BM
WT mice /KO BM
KO mice /KO BM

Figure. 5